Cerebral Cortex Advance Access published March 25, 2010

Cerebral Cortex
doi:10.1093/cercor/bhq040

Enhanced Infragranular and Supragranular Synaptic Input onto Layer 5 Pyramidal Neurons in a Rat Model of Cortical Dysplasia

Julia Brill and John R. Huguenard

Department of Neurology and Neurological Sciences, Room M016, Stanford University School of Medicine, 300 Pasteur Drive, Stanford, CA 94305, USA

Address correspondence to Julia Brill, Department of Neurology and Neurological Sciences, 300 Pasteur Drive, Stanford, CA 94305. Email: jbrill@stanford.edu

Cortical dysplasias frequently underlie neurodevelopmental disorders and epilepsy. Rats with a neonatally induced cortical microgyrus [freeze-lesion (FL)], a model of human polymicrogyria, display epileptiform discharges in vitro. We probed excitatory and inhibitory connectivity onto neocortical pyramidal neurons in layers 2/3 and 5 of postnatal day 16–22 rats, approximately 1–2 mm lateral of the lesion, using laser scanning photostimulation (LSPS)/glutamate uncaging. Excitatory input from deep and supragranular layers to layer 5 pyramidal cells was greater in FL cortex, while no significant differences were seen in layer 2/3 cells. The increased input was due to a greater number of LSPS-evoked excitatory postsynaptic currents (EPSCs), without differences in amplitude or kinetics. Inhibitory input was increased in a region-specific manner in pyramidal cells in FL cortex, due to an increased inhibitory postsynaptic current (IPSC) amplitude. Connectivity within layer 5, parts of which are destroyed during lesioning, was more severely affected than connectivity in layer 2/3. Thus, we observed 2 distinct mechanisms of altered synaptic input: 1) increased EPSC frequency suggesting an increased number of excitatory synapses and 2) higher IPSC amplitude, suggesting an increased strength of inhibitory synapses. These increases in both excitatory and inhibitory connectivity may limit the extent of circuit hyperexcitability.

Keywords: freeze-lesion, laser scanning photostimulation, polymicrogyria, synaptic excitation, synaptic inhibition

Introduction

Cortical dysplasias result from a developmental disruption of neuronal migration. They comprise a wide range of conditions that are often associated with mental retardation, cognitive deficits, and epilepsy (reviewed e.g., Crino 2004; Sisodiya 2004; Leventer et al. 2008; Pang et al. 2008). Polymicrogyria is a form of neocortical dysplasia characterized by the presence of small gyri and sulci associated with an abnormal 4-layered structure and absence of deep layers. Surrounding cortical areas show normal lamination (Harding and Copp 1997). Formation of the microgyri is thought to be caused by ischemia/hypoxia during the second gestational trimester, viral infections, or mutations affecting cortical development (Barkovich and Lindan 1994; Barkovich et al. 1995).

Humans with polymicrogyria frequently have intractable epilepsy. Rats with a single experimental microgyrus (Dvorak and Feit 1977; Rosen et al. 1992), induced by a neonatal freeze-lesion (FL, see Methods), do not have spontaneous epileptiform activity in vivo (Kellinghaus et al. 2007) but exhibit a decreased seizure threshold with certain experimental paradigms (Scantlebury et al. 2004; but see Kellinghaus et al. 2007). Cortical slices display a decreased threshold for the generation of polysynaptic ("epileptiform") activation for a distance of up to several millimeter lateral of the lesion. Epileptiform activity can be generated outside the lesion itself (Jacobs et al. 1996) and is dependent on α-amino-3-hydroxyl-5-methyl-4-isoxazole-propionate (AMPA) receptor activation (Luhmann and Raabe 1996; Luhmann et al. 1998).

Multiple changes in protein expression occur in the affected and the contralateral hemisphere. Specific results differ depending on the region, age, or methodology, that is, expression levels of a particular interneuronal marker versus number of neurons expressing that marker (Jacobs et al. 1996; Hablitz and DeFazio 1998; Rosen et al. 1998; Schwarz et al. 2000; Patrick et al. 2006) or neurotransmitter receptor expression versus binding sites (Zilles et al. 1998; Redecker et al. 2000; Hagemann et al. 2003). These changes are also reflected in altered electrophysiological characteristics of neurons. In layer 5 pyramidal cells, the number of spontaneous and miniature EPSCs is increased, while spontaneous and evoked, but not miniature, IPSCs are larger (Jacobs and Prince 2005). Larger miniature IPSCs have been reported in layer 2/3 pyramidal cells (DeFazio and Hablitz 1999).

Here, we investigated excitatory and inhibitory connectivity onto layer 2/3 and 5 pyramidal cells in the hyperexcitable zone approximately 1 mm lateral of the microgyrus and in homotopic cortex of sham-operated controls. Laser scanning photostimulation (LSPS) is a method that allows rapid, transient, and focal release of glutamate onto slice preparations. Glutamatergic stimulation of neuronal soma, but not axons or dendrites, leads to action potential generation and thus allows for the localization of somata of the synaptic inputs. It is then possible to discriminate whether synaptic inputs are stronger (changes in postsynaptic current [PSC] amplitude) or more frequent (changes in PSC number and/or spots from which PSCs are evoked), which can provide mechanistic information regarding FL-induced presynaptic and/or postsynaptic changes and resultant hyperexcitability.

Materials and Methods

Induction of Experimental Microgyri

All experiments were carried out according to protocols approved by the Stanford Institutional Animal Care and Use Committee. For our studies, experimental microgyri were induced in Sprague–Dawley rat pups by freeze-lesioning as described previously (Jacobs et al. 1996). In this model, FLs can be induced at either P0 or P1—lesioning at later time points does not result in the formation of a 4-layered microgyrus (Dvorak et al. 1978). We chose to restrict lesioning to P0 to minimize response variability. Briefly, pups were anesthetized by hypothermia, the skull was exposed, and a 5 × 2-mm metal probe cooled to −50 to −60 °C was placed onto the exposed skull above the right

somatosensory cortex (1 mm from, and parallel to, midline, between lambda and bregma) for approximately 5 s. Controls were sham-operated littermates (with the probe warmed to room temperature). After surgery, the scalp was sutured; pups were warmed and returned to the dam.

Slice Preparation

Experiments were performed in P16–22 rats, since in vitro epileptiform activity is first evident around P12 (Jacobs et al. 1996) and crucial developmental changes in fast glutamate receptor expression are largely complete by P15 (Brill and Huguenard 2008). Average ages for control and FL rats used were P18.2 and P17.7, respectively. Typically, slices were prepared from a control rat and a free-lesioned littermate on the same day in parallel. Animals were deeply anaesthetized using 50 mg/kg sodium pentobarbital, and brains were removed and immediately transferred to ice cold sucrose solution containing, in mM: 234 sucrose, 11 glucose, 24 $NaHCO_3$, 2.5 KCl, 1.25 NaH_2PO_4, 2 $MgSO_4$, and 0.5 $CaCl_2$, equilibrated with a 95–5% mixture of O_2 and CO_2. In total, 350–400 μm coronal neocortical slices were sectioned on a VT 1000S vibratome (Leica) at 4 °C in sucrose solution and transferred into a holding chamber filled with artificial cerebrospinal fluid (ACSF; in mM: 126 NaCl, 26 $NaHCO_3$, 2.5 KCl, 1.25 NaH_3PO_4, 2 $CaCl_2$, 2 $MgCl_2$, 10 glucose, equilibrated with 95% O_2/5% CO_2, pH 7.4). After a recovery period of 1 h at 32 °C, the holding chamber containing the slices was removed from the water bath and allowed to cool to room temperature before recordings were obtained.

Focal Photolysis of Caged Glutamate/Laser Scanning Photostimulation

Focal photolysis of caged glutamate was performed as previously described (Deleuze and Huguenard 2006; Jin et al. 2006; Brill and Huguenard 2009). A pulsed 355 nm UV laser beam (DPSS Lasers) was directed into the back aperture of the 5 or ×63 microscope objective and was controlled with mirror galvanometers (Model 6210; Cambridge Technology) using a locally developed software program. The beam half-width was approximately 130 μm at ×5. Focal photolysis of Montreal Neurological Institute (MNI)-caged glutamate (Tocris; 100 μM) was triggered by 50 mW UV light pulses (300–800 μs). MNI-caged glutamate was supplied in a 30-mL recirculating bath solution. Typically, the bath solution was exchanged after 3–4 h or sooner if significant rundown of direct responses was detected. Since MNI-glutamate quality varied somewhat between batches and aliquots, stimulation intensity was determined at the start of each experimental day in one control slice by uncaging directly onto the soma of a control layer 5 pyramidal cell that was recorded either in cell-attached or in voltage clamp mode. The minimum laser pulse duration needed to evoke a spike (cell-attached mode) or a direct current of 200–300 pA (voltage clamp mode) was determined, and 1.2× this duration was used in subsequent recordings.

Electrophysiological recordings

Slices were transferred to a recording chamber and constantly superfused with oxygenated ACSF at a rate of approximately 2 mL/min. Experiments were conducted at room temperature (23–25 °C) to avoid excessive evaporation of the relatively small volume (30 mL) of recirculating ACSF. All cells recorded were located in primary somatosensory cortex in limb and trunk areas lateral of the microgyrus in FL cortex. Cortical layers were identified visually from an overview image obtained with a ×5 objective and neurons were visualized with a ×63 objective using differential contrast optics with an Axioskop 2 FS microscope (Zeiss). Pyramidal cells were identified based on their large size, tear-shaped morphology, and thick apical dendrite. Cells were routinely filled with 0.3% w/v biocytin, for post recording recovery to confirm their identity. Whole cell and cell-attached recordings were obtained using borosilicate glass electrodes with a tip resistance of 2–4 MΩ. The pipette solution used for most voltage clamp recordings (connectivity mapping and short term plasticity) and cell-attached recordings (excitation profiles) contained, in mM: 130 Cs-gluconate, 8 CsCl, 10 HEPES (4-(2-hydroxyethyl)-1-piperazineethanesulfonic acid), 4 ethyleneglycol-bis(2-aminoethylether)-*N,N,N',N'*-tetra acetic acid (EGTA), and 0.01 QX314 [*N*-(2,6-dimethylphenylcarbamoylmethyl) triethylammonium bromide], pH 7.3 adjusted with CsOH (290 mOsm). For all current clamp recordings and voltage clamp recordings used to determine intrinsic excitability, the following internal solution was used, in mM: 120 K-gluconate, 11 KCl, 1 $MgCl_2$, 1 $CaCl_2$, 10 HEPES, 10 EGTA, and pH 7.3 adjusted with KOH. N-methyl-D-aspartate (NMDA) receptor mediated currents were blocked by 50 μM D-AP5 (Ascent Scientific). Only recordings in which the series resistance was <25 MΩ and changed <30% during the recording were included in the data analysis, and no series resistance compensation was employed. Membrane potentials were corrected for a liquid junction potential of 20 mV, and all voltages given subsequently include liquid junction potential correction. Signals were amplified with a Multiclamp 700A amplifier, sampled at 10 kHz, filtered at 3 kHz, acquired using a Digidata 1320A digitizer, and analyzed using pClamp9 (all Molecular Devices).

Synaptic Input Maps

Maps consisted of 143–182 points spanning all cortical layers with a grid spacing of 90–100 μm. Points were stimulated in a pseudorandom pattern designed to minimize sequential activation of adjacent grid points, with 5 s between stimuli. To isolate excitatory postsynaptic current (EPSC) input, maps were recorded at a holding potential of −65 mV, near the chloride equilibrium potential, where GABAergic activation results in minimal outward currents that do not interfere with the detection of the much larger inward glutamatergic currents. In this way, direct and synaptic excitation could be simultaneously monitored in the same map. Direct glutamatergic currents are recorded when glutamate is released onto the recorded cell (Brill and Huguenard 2008). These responses consistently have an onset latency of <3 ms and were distinguished from EPSCs on that basis. We excluded sweeps in which direct activation exceeded 100 pA, such that it would interfere with detection of synaptic responses. Subsequently, maps were recorded at −5 mV, close to the reversal potential for AMPA receptor mediated currents, to isolate IPSCs. At −5 mV, glutamatergic activation results in small inward currents, which can be readily distinguished from outward GABAergic currents. To construct maps, we determined the cumulative amplitude of PSCs with onset latencies of 5–50 ms (EPSCs) and 2–50 ms (IPSCs) after the stimulus for each sweep. The cumulative amplitude is the sum of the amplitudes of all PSCs recorded within the detection time window and therefore represents a compound measure of event frequency and amplitude. We used a relatively short time window to avoid confounding effects of polysynaptic activation, whose contribution to overall synaptic responses was additionally minimized by blockade of NMDA receptors. PSCs were detected using locally written software and validated by visual examination of raw traces. We then corrected the cumulative amplitude for the expected spontaneous activity in the equivalent time window. Spontaneous activity was determined for each cell for 1.5 s/sweep during the interstimulus intervals starting 500 ms after each photostimulation. Typically, 2 EPSC and inhibitory postsynaptic current (IPSC) maps were obtained using the same grid, and the results were averaged. Occasional sweeps in which clear polysynaptic epileptiform currents were detected were excluded from analysis. Those were high amplitude (>100 pA), polyphasic, long lasting (>50 ms), and long-latency (20–100 ms) events. If >5 such events were detected in a given cell, it was excluded from further analysis. Averaged maps derived from all individual maps (see Figs 5–7) were obtained by using exact measurements of the x and y distances of each stimulation point from the reference point (soma or layer 1/2 border) and then binning these at 50 μm intervals. Smooth contours were derived by linear interpolation between 50 μm bins, but we did not interpolate between individual data points.

Direct Excitation Profiles

Direct excitation profiles were constructed by recording action potentials elicited by LSPS in cell-attached mode and scanning areas within 200–300 μm of the recorded cell using 50–75 μm grids. After recording one map in cell-attached mode, we typically acquired whole-cell configuration and recorded the same map again in voltage clamp mode. We then matched success or failure of action potential generation to the corresponding direct glutamatergic currents.

Intrinsic Excitability

Spike frequency, action potential half-width, and threshold were measured in current clamp mode using hyperpolarizing and depolarizing currents (0.5 s, –150 to 300 pA, 50 pA steps). Resting membrane potential was determined 2–3 min after establishing whole-cell configuration. Membrane capacitance, input resistance, and access resistance were determined in voltage clamp mode from averaged responses to 30 voltage steps (100 ms, +10 mV) from a holding potential of –65 mV, as described previously (Destexhe et al. 1996). Hyperpolarization-activated cationic current (I_h) was determined from the response to a hyperpolarizing voltage step (1 s, –65 to –80 mV) by measuring the difference between the holding current at the beginning and at the end of the step.

Short-Term Plasticity

Paired pulse ratios and ratios of the eighth to the first pulse were determined at a holding potential of –65 mV in the presence of NMDA and $GABA_A$ receptor blockers. EPSCs were evoked by electrical stimulation using a concentric bipolar electrode (75 μm diameter; CB-XRC75, Frederick-Haer), which was positioned on-column close to the recorded cell in the same layer. Synaptic activity was evoked by delivering trains of 8 current pulses (100–500 μA, 100 μs) at interpulse intervals of 25, 50, 75, 100, 250, 500, and 1000 ms. Stimulation intensities were selected to correspond to approximately 2× threshold for a detectable response.

Histology

Brains were removed and sectioned into 400 μm slices as described for electrophysiological experiments and subsequently transferred into ice-cold fixative containing 4% paraformaldehyde in 0.1 M phosphate buffer, pH 7.4, cryoprotected by immersion in 30% sucrose in phosphate-buffered saline for 1–2 h and resectioned at 50 μm. Sections were then Nissl stained according to standard procedures. Layers 1–6 were identified from Nissl-stained sections or brightfield images obtained during recordings (example shown in Fig. 1*B,C*). In brightfield images, layer 1 appears smooth and bright, layer 4 appears darker than the adjoining layers 2/3 and 5a, and layer 5a is brighter than layer 5b. Layer 6 tends to appear brighter than layer 5b, but a clear border could not always be determined.

Statistics

Data are given as average ± standard error of the mean. Statistical comparisons between 2 groups were calculated using unpaired Student's *t*-tests, with *P* values < 0.05 indicating significance.

Results

Generation of Monosynaptic Excitatory and Inhibitory Input Maps in Pyramidal Cells

Layer 2/3 and 5 pyramidal cells 0.5–1.0 mm lateral to the edge of the microgyrus or equivalent areas in sham-operated rats aged P16 to P22 were used in this study (Fig. 1*A*). The mapped area in FL cortex had normal lamination, and the laminar thickness did not differ from that in sham-control cortex (Fig. 1*B–D*). The layer dimensions were similar to previously reported values (Hutsler et al. 2005). We mapped excitatory inputs using a holding potential of –65 mV, which is close to the chloride equilibrium potential of –68 mV. Inhibitory input maps were acquired at –5 mV, close to the reversal potential for AMPA-receptor mediated currents of 0 mV. As described previously (Brill and Huguenard 2009), inhibitory responses were classified into short- and long-latency events (slIPSCs, 2–10 ms vs. rlIPSCs, 10–50 ms post LSPS stimulus, respectively) such that separate maps could be extracted for both types of inhibitory events. Maps typically spanned approximately

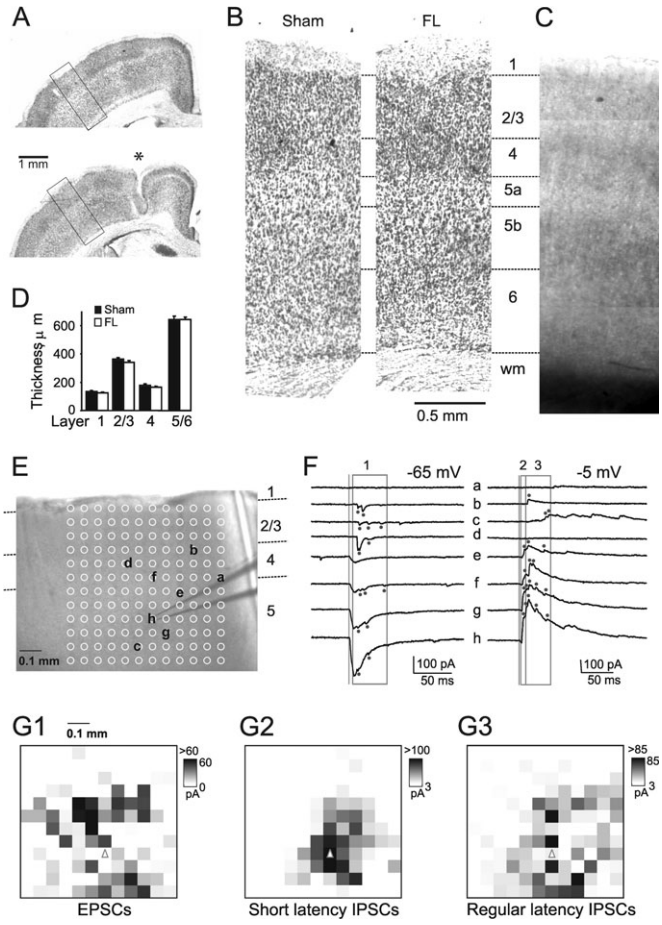

Figure 1. Generation of monosynaptic input maps using LSPS. (*A*) Nissl-stained sections from control (upper) and FL (lower) cortex. The lesion is marked with an asterisk. Black rectangles mark area shown in (*B*). (*B*) Enlarged area indicated by rectangles in (*A*) from control (left) and FL (right) cortex. Approximate layer borders are indicated by dashed lines. Numbers indicate layers; wm, white matter. Cortical lamination does not differ systematically between control and FL. (*C*) Examples of cortex as view in live slices in the recording chamber. Midline is toward the left. Note that layers 1, 2/3, 4 and underlying white matter are well resolved in the Nissl-stained sections and can also be clearly distinguished in the live slice. The border between 5 and 6 is ambiguous in the live slices, and therefore, the laminar thickness analysis in (*D*) combines them and represents the composite depth as layer 5/6. Scale bar in (*B*) applies to (*C*). (*D*) Thickness of cortical layers as estimated from overview images such as the ones shown in (*A*) for 25 slices each in control and FL cortex 1.5–2.5 mm from the central sulcus. There were no significant differences between FL and control cortex. (*E*) Example input map grid of a layer 5 cell in FL cortex. White circles indicate the LSPS grid; some spots are marked with lower case letters. The pipette tip indicates the position of the soma, approximately at spot "h". (*F*) Example traces recorded at −65 mV (left) and −5 mV (right) at the locations indicated by lowercase in (*E*). The gray line corresponds to the time of LSPS stimuli; circles indicate evoked PSCs. Boxes delineate detection windows for EPSCs (box 1 on left, 10–50 ms), box 2 (right) outlines the detection window used to detect slIPSCs (2–10 ms), box 3 adjacent to box 2 outlines the detection window for rlIPSCs (10–50 ms). Selected traces are ordered to have minimum overlap and to show a progression from no to high LSPS-evoked activity. (*G*) Input maps generated from the cell shown in (*E* and *F*). (*G1*) EPSCs (box 1 from *D*); (*G2*) slIPSCs (box 2 from *D*); and (*G3*) rlIPSCs (box 3 from *D*). *x*- and *y*-axes correspond to the grid in (*C*); grayscale values represent the cumulative amplitude of evoked events (number of events times their average amplitude), going from white to black (low to high cumulative amplitude). The triangle indicates the location of the recorded cell's soma.

1–1.3 mm^2, with a grid spacing of 90–100 μm, and 2 replicates each were generated at –65 mV and –5 mV. We limited the likelihood of evoking polysynaptic activation by blocking NMDA receptors. There is no evidence for significant numbers

of silent, that is, NMDA receptor only, glutamatergic synapses in neocortex after postnatal day 16 (Isaac et al. 1997; Rumpel et al. 2004; Busetto et al. 2008), so NMDA receptor block will not interfere with the identification of glutamatergic input patterns. We also used a relatively short detection window for synaptic activation (50 ms after LSPS), which further reduces inclusion of late polysynaptic PSCs. Figure 1*E* shows an example map grid for a recorded layer 5 pyramidal cell in FL cortex with the mapping grid, and representative excitatory and inhibitory synaptic inputs at indicated grid points are shown in Figure 1*F*. Figure 1*G* shows the overall excitatory and inhibitory maps generated from that cell.

Equivalent Direct Activation and Intrinsic Excitability of Pyramidal Cells in FL and Control Cortex

When glutamate is uncaged onto the soma or dendrites of the recorded cell, AMPA receptors are activated directly. Sufficiently large direct glutamatergic activation can cause suprathreshold depolarization. To assess whether the spatial profile of LSPS-evoked action potential generation differed in pyramidal cells in layers 2/3 and 5 of FL and control cortex, we generated direct excitation profiles. To that end, maps centered on the recorded cell spanning approximately 400–500 μm^2 with grid spacings of 50–75 μm were scanned using LSPS, and action potentials were recorded in cell-attached mode (an example is shown in Fig. 2*A*). Since cell-attached recordings do not perturb the intracellular environment, they are well suited to study action potential generation as a result of focal glutamate release. The probability for generating at least one spike was calculated and the data sorted into 50 μm bins according to the distance between the soma and the uncaging site (Fig. 2*B*). There was no significant difference in the spike probability between cells from FL and control cortex in layer 2/3 (Fig. 2*B*, left panel; control: $n = 10$; FL: $n = 7$) or layer 5 (Fig. 2*B*, right panel; control: $n = 10$; FL: $n = 8$). Likewise, there were no differences between cells from FL and control cortex in the number of spikes per "hotspot," that is, grid points from which spikes were evoked (layer 2/3; control: 1.01 ± 0.01 spikes/hotspot, FL: 1.09 ± 0.07 spikes/hotspot, $P = 0.21$. Layer 5; control: 1.43 ± 0.21 spikes/hotspot, FL: 1.43 ± 0.18 spikes/hotspot, $P = 1.00$; Fig. 2*D2*) and in the median distance of hotspots from the recorded cell's soma (layer 2/3; control: 91.9 ± 10.5 μm, FL: 77.8 ± 13.1 μm, $P = 0.41$. Layer 5; control: 89.7 ± 8.8 μm, FL: 97.9 ± 9.5 μm, $P = 0.53$; Fig. 2*D3*). All action potentials were evoked within 250 μm of the recorded cell's soma, indicating that they were the result of activation via glutamate released directly onto the recorded cell rather than the result of network activation leading to suprathreshold EPSPs. In some cells, whole-cell configuration was established after cell-attached recordings so that the same LSPS map could be repeated in voltage clamp mode (cesium-gluconate based internal solution with QX-314 to block sodium channels) and the amplitude of direct glutamatergic currents corresponding to spike generation could be determined (Fig. 2*C*). We found that the equivalent minimum current needed to evoke spikes was significantly larger in layer 2/3 cells compared with layer 5 cells, which is probably due to the fact that layer 2/3 pyramidal cells have a more negative resting membrane potential than layer 5 cells (see Table 1). However, there were no differences within each layer between cells from FL and control cortex (smallest current corresponding to spike generation: layer 2/3; control: 256 ± 29 pA, $n = 9$; FL: 264 ± 34 pA, $n = 11$, $P = 0.85$. Layer 5; control: 101 ± 19 pA, $n = 10$; FL: 105 ± 14 pA, $n = 6$, $P = 0.88$; Fig. 2*D1*). Thus, we conclude that there are no significant differences in LSPS-evoked direct excitation of pyramidal cells in FL versus control cortex.

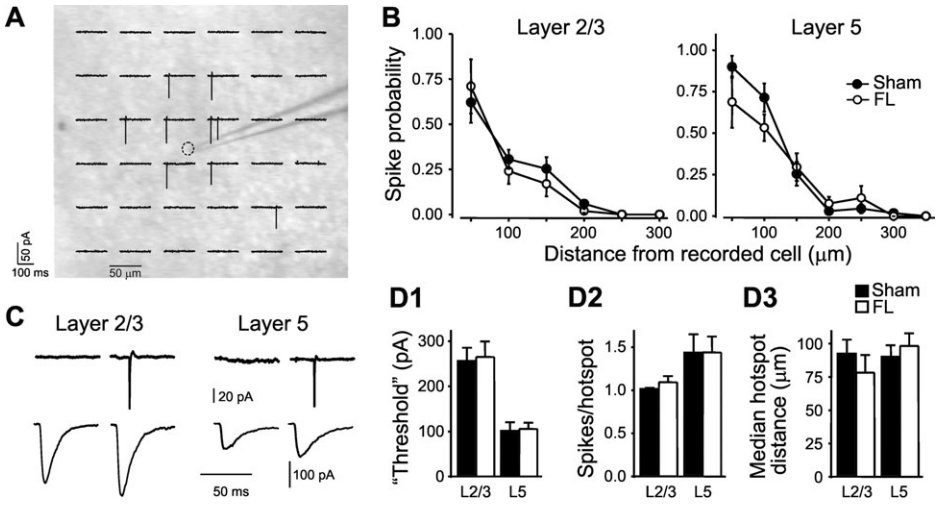

Figure 2. Direct excitation profiles do not differ in FL and control cells. (*A*) Example map of LSPS-evoked action potentials recorded in cell-attached mode in a layer 5 pyramidal cells in sham-control cortex. Traces are superimposed onto the image of the slice to indicate the approximate location of LSPS and the location of the recorded cell's soma (indicated by the pipette tip). (*B*) Comparison of spike probability after LSPS in control and FL cortex in layer 2/3 cells (left panel; control: $n = 10$; FL: $n = 7$) and 12 layer 5 cells (right panel; control: $n = 10$; FL: $n = 8$). The probability to evoke a spike for each cell was averaged into 50 μm bins according to the distance between stimulation site and the soma. There were no significant differences between cells from sham-control and FL cortex. (*C*) Current responses (bottom traces) to equivalent stimuli producing just subthreshold and just suprathreshold depolarizations (top traces) in a layer 2/3 and a layer 5 pyramidal cells in control cortex. The layer 2/3 cell requires a much larger amplitude equivalent current to reach action potential threshold. (*D*) Summary of direct excitation parameters. (*D1*) Average equivalent currents for suprathreshold depolarization in layer 2/3 (control: $n = 9$, FL: $n = 11$) and layer 5 pyramidal cells (control: $n = 10$, FL: $n = 6$). Although "threshold currents" differed significantly between layers 2/3 and 5, there were no statistical differences between cells from FL and control cortex in either layer. (*D2*) Average spikes per hotspot (i.e., LSPS site from which action potentials were evoked) for the same set of cells shown in (*B*). There were no significant differences between cells from FL and control cortex. (*D3*) Median distance of hotspots from the recorded cells' soma, same set of cells as those shown in (*B*). There were no significant differences between cells from FL and control cortex.

Next, we assessed the amplitude of the direct current generated in pyramidal cells from which synaptic connectivity maps were constructed. Direct non-synaptic currents are evoked during acquisition of synaptic input maps when glutamate is released directly onto the recorded cells' soma or dendrites. Direct currents can be distinguished from synaptic activation by their short onset latency (<3 ms compared with >5 ms for glutamatergic synaptic currents) and longer rise and decay kinetics. Figure 3*A1,A2* shows direct currents from a layer 2/3 and a layer 5 cell, respectively, in control cortex, and Figure 3*B1,B2* shows direct excitation maps generated from these cells. Direct glutamatergic currents were centered on the soma of the recorded cell and their amplitude decreased with increasing distance from the soma. We averaged direct activation from all cells recorded (12 cells each in control and FL layer 5, 13 cells each in control and FL layer 2/3) and quantified average direct excitation amplitudes in 50 μm bins according to the distance between the soma and the uncaging site (Fig. 3*C1,C2*). No significant differences were seen in direct response amplitudes in pyramidal cells from FL cortex from which subsequent synaptic input maps were generated, indicating that direct AMPAergic currents do not differ in pyramidal cells from FL and control cortex and that slices from FL and control animals received equivalent LSPS stimulation.

To determine whether changes in intrinsic membrane properties should be taken into consideration when interpreting synaptic input maps, we measured input resistance, membrane capacitance, resting membrane potential, hyperpolarization-induced cation current (I_h), spiking frequency in response to depolarizing current injections, threshold for action potential generation, and action potential shape in layer 2/3 and 5 pyramidal cells. We found no significant differences between cells from FL and control cortex in any of the parameters tested (Table 1).

Table 1
Intrinsic membrane properties

	Layer 2/3		Layer 5		Layer 2/3 versus layer 5
	Sham (n = 16)	FL (n = 16)	Sham (n = 16)	FL (n = 16)	
Resting potential (mV)	−67.4 ± 0.8	−66.5 ± 0.5	−56.6 ± 0.8	−55.4 ± 0.8	****
Input resistance (MΩ)	434 ± 39	367 ± 21	230 ± 22	313 ± 36	—
Capacitance (pF)	336 ± 14	361 ± 11	593 ± 40	530 ± 26	****
Spike frequency (Hz @ 200 pA)	19.3 ± 0.6	19.9 ± 0.8	15.4 ± 1.3	16.5 ± 0.8	*
AP #1 half width (ms)	1.72 ± 0.6	1.74 ± 0.06	1.48 ± 0.04	1.51 ± 0.04	—
AP #3 half width (ms)	3.21 ± 0.28	2.96 ± 0.17	2.00 ± 0.14	2.09 ± 0.12	***
AP #1 maximum (mV)	52.5 ± 1.0	53.9 ± 1.3	57.3 ± 1.3	56.4 ± 1.1	—
AP #3 maximum (mV)	36.5 ± 2.7	38.5 ± 1.6	40.5 ± 3.4	41.6 ± 2.0	—
AP threshold (mV)	−36.3 ± 0.5	−37.4 ± 0.5	−36.2 ± 0.3	−36.6 ± 0.6	—
I_h at −80 mV (pA)	9.2 ± 2.2	7.5 ± 2.3	96.1 ± 11.6	84.0 ± 11.2	****

Note: AP, action potential. Intrinsic membrane properties of pyramidal cells in layer 2/3 and 5. There were no significant differences between cells of FL and control cortex within each layer. There were significant differences between layer 2/3 and 5 pyramidal cells (right column). *$P < 0.05$; ***$P < 0.001$; ****$P < 0.0001$; —, not significant, $P > 0.1$. P values were determined for comparisons between control cells, but if no significant difference was detected between cells from FL cortex, the comparison was listed as not significant.

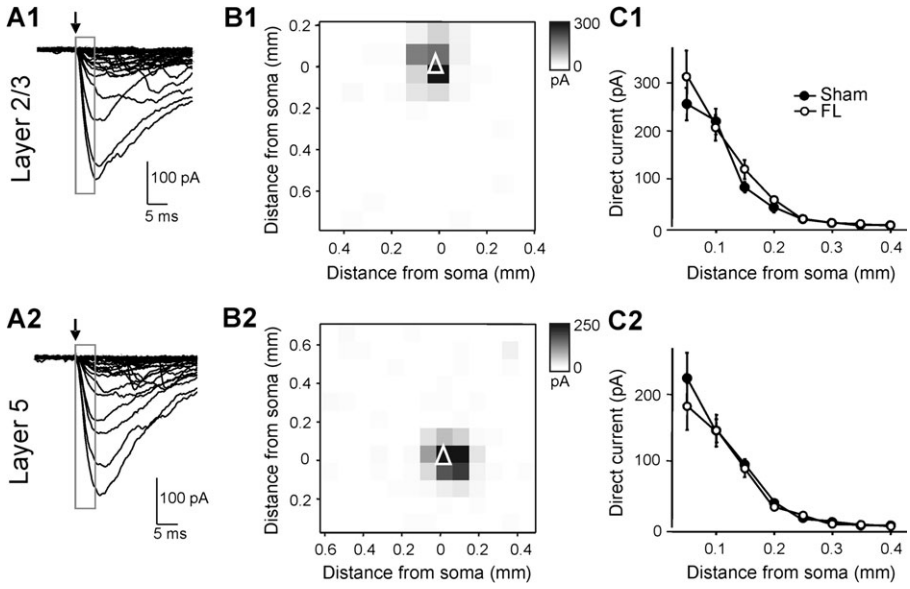

Figure 3. Direct glutamatergic currents do not differ in FL and control cells. (*A*) Example traces from a layer 2/3 (*A1*) and a layer 5 (*A2*) pyramidal cells in sham-operated control cortex recorded at −65 mV, focusing on the time immediately following the stimulus (indicated by arrow). Currents rising within 3 ms of the stimulus, as indicated by the gray rectangles, were evoked by direct activation of glutamate receptors on the recorded neurons. (*B*) Maps representing the amplitude of direct currents generated from the cells shown in (*A*). The open white triangles indicate position of the soma in layer 2/3 (*B1*) and layer 5 (*B2*). Direct currents were evoked perisomatically and their amplitude decreased with increasing distance from the soma. (*C*) Comparison of direct currents evoked in 13 layer 2/3 cells (*C1*) and 12 layer 5 cells (*C2*) each in control and FL cortex. Current amplitudes for each cell were averaged into 50 μm bins according to the distance between stimulation site and the soma. There were no significant differences between direct glutamatergic currents in cells from control and FL cortex.

Lastly, we determined whether alterations in short-term plasticity in pyramidal cells of FL cortex might contribute to hyperexcitability. EPSCs in layer 2/3 and 5 pyramidal cells were evoked by trains of 8 electrical stimuli at interstimulus intervals of 25–1000 ms (Fig. 4*A*). Again, we found no significant differences between cells from FL and control cortex in either layer in paired pulse ratios (Fig. 4*B1,B2*) or in the ratio of the eighth over the first EPSC (Fig. 4*C1,C2*). Thus, short-term plasticity, which reflects in part release probability, was unaffected in FL cortex. This indicates that hyperexcitability in FL cortex is likely due to either postsynaptic changes or axonal sprouting, which we tested for in the following experiments.

Layer-Specific Changes in Excitatory Input onto Pyramidal Cells in FL Cortex

At the time of freeze-lesioning (P0), layer 5 cells have already migrated into the cortical plate and are obliterated at the site of the lesion (Rosen et al. 1992). Layer 2/3, on the contrary, has not yet formed, and an aberrantly structured, but contiguous layer 2/3 forms across the lesion. Layer 2/3 and 5 might therefore display different developmental and structural plasticity to compensate.

Excitatory input maps for pyramidal cells in FL and control cortical layers 5 (12 cells each) and 2/3 (13 cells each) were acquired. Inputs coming from different cortical depths were quantified by aligning maps from each cell at the layer 1/layer 2 border (position 0 on the *y*-axes). The composite maps in Figure 5*A1,A2* show the averaged cumulative evoked EPSC amplitude (i.e., the sum of the amplitudes of EPSCs at each stimulation site, a combined measure of the number and strength of inputs) in layer 2/3 and 5 cells from control and FL cortex. Figure 5*B1,B2* shows vertical excitation profiles, which depict the average activation per spot within each row of the mapping grid. Figure 5*C* shows the averaged cumulative amplitude per grid spot of EPSCs originating in layers 2/3, 4/5a, and 5b/6 onto layer 2/3 (Fig. 5*C1*) and layer 5 (Fig. 5*C2*). Inputs from layers 4 and 2/3 to layer 2/3 cells were not significantly different from control. Layer 5 cells in FL cortex however received significantly stronger inputs from layers 5b/6 (control: 5.46 ± 1.11 pA/spot; FL: 10.73 ± 2.26 pA/spot; $P < 0.05$) and from layer 2/3 (control: 4.23 ± 0.75 pA/spot; FL: 7.56 ± 1.53 pA/spot; $P < 0.05$). Lateral excitation profiles, generated by averaging inputs within each column of the mapping grid, are shown in Figure 5*E1,E2* for layer 2/3 and 5, respectively, fitted to Gaussian distributions. Excitation half-width do not differ, indicating that excitatory inputs onto cells from control and FL cortex have the same columnar profile. Globally, layer 5 pyramidal cells in FL cortex received more excitatory input per stimulated spot than cells in sham-operated control cortex (control: 4.23 ± 0.56 pA/spot, FL: 7.36 ± 0.77 pA/spot; $P < 0.01$; Fig. 5*D2* and Table 2). Overall excitatory input to layer 2/3 pyramidal cells did not differ statistically between FL and control cortex (control: 3.04 ± 0.58 pA/spot, FL: 3.92 ± 0.65 pA/spot; $P = 0.32$; Fig. 5*D1* and Table 2).

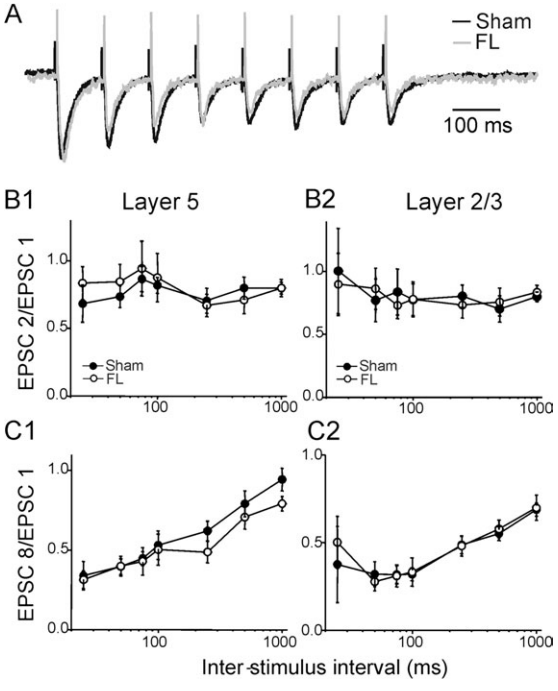

Figure 4. Short-term plasticity of EPSCs is similar in FL and control cells. (*A*) Example EPSC responses to trains of 8 electrical stimuli (100 ms interstimulus interval, −65 mV holding potential) in layer 5 pyramidal cells from sham-control (black trace) and FL cortex (gray trace). (*B*) Paired pulse ratios (EPSC 2:EPSC 1 in each 8-pulse train) measured at interstimulus intervals of 25, 50, 75, 100, 250, 500, and 1000 ms in layer 5 (*B1*) and layer 2/3 (*B2*) pyramidal cells of control (filled circles; layer 2/3, $n = 9$; layer 5, $n = 7$) and FL (open circles; layer 2/3, $n = 9$; layer 5, $n = 8$) cortex. There were no significant differences between cells from control and FL cortex. (*C*) Ratios of the eighth to the first EPSC in the same 8-pulse trains analyzed in (*B*). The EPSC 8:EPSC 1 ratios at interstimulus intervals between 25 and 100 ms show larger depression than the EPSC 2:EPSC 1 ratios (*B*), but there were no significant differences between cells from control and FL cortex.

Number, but Not Amplitude, of Evoked and Spontaneous EPSCs Is Increased in Layer 5 Pyramidal Cells of FL Cortex

The synaptic input maps generated in this study quantify the cumulative amplitude within the detection window, that is, a combined measure of event amplitude and frequency. As noted above, intrinsic excitability, direct excitation, and short-term plasticity were not affected in FL cortex. Thus, changes in cumulative amplitude of synaptic inputs could be due to altered numbers of synapses, which would lead to changes in the numbers of LSPS-evoked EPSCs or to altered strength of individual connections, which would lead to larger EPSC amplitudes, or both. In order to discriminate between these possibilities, we quantified amplitude and number of LSPS-evoked EPSCs (i.e., EPSCs recorded between 5 and 50 ms after the laser pulse, corrected for spontaneous activity). We found no differences in the amplitude and kinetics of LSPS-evoked EPSCs in pyramidal cells of FL and control cortex (Table 2). By contrast, the number of LSPS-evoked EPSCs in layer 5 pyramidal cells was increased in FL cortex (control: 0.55 ± 0.07 EPSCs/stimulated spot, FL: 0.82 ± 0.11 EPSCs/spot, $P < 0.05$; Fig. 5*F2*, Table 2). The fraction of stimulation spots in layer 5b/6 from which EPSCs were elicited in layer 5 cells was increased in FL cortex, especially from the deepest half (control: EPSCs elicited from 41.9 ± 4.1% of stimulation sites, FL: 55.5 ± 5.0%; $P < 0.05$, data not shown). This indicates the possibility of a greater number of presynaptic neurons in FL cortex. The number of LSPS-evoked EPSCs in layer 2/3 pyramidal cells was not significantly different from control (control: 0.62 ± 0.06 EPSCs/spot, FL: 0.77 ± 0.06 EPSCs/spot, $P > 0.5$; Fig. 5*F1*; Table 2).

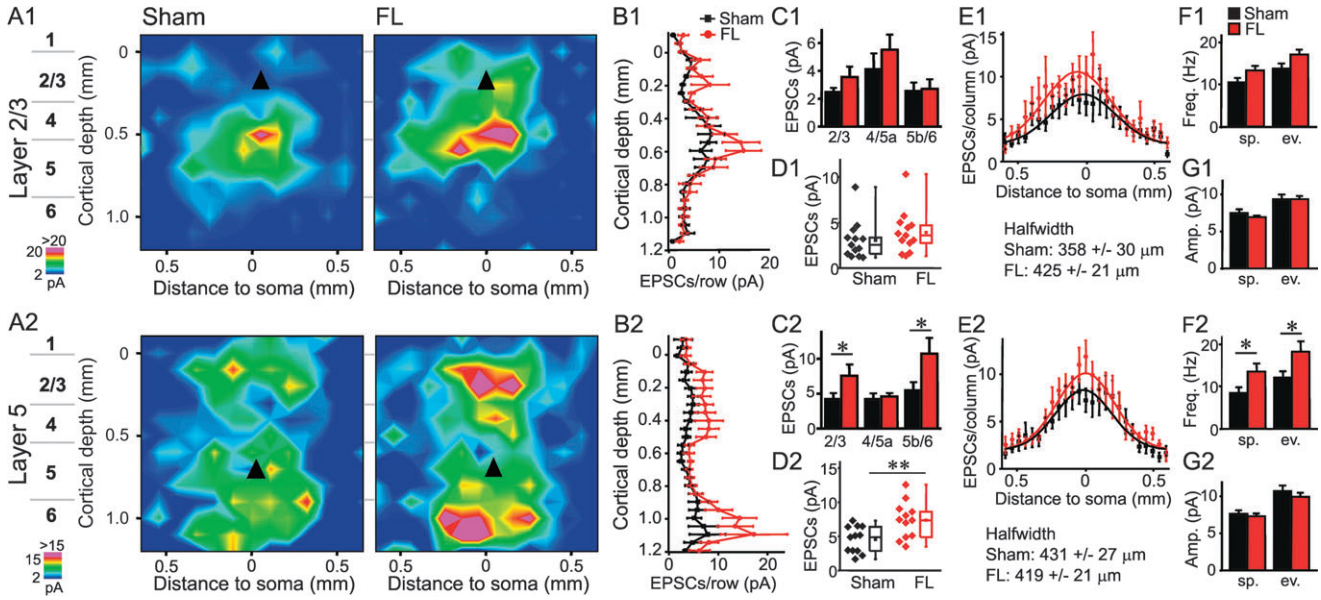

Figure 5. Increased excitatory input onto layer 5, but not layer 2/3 cells in FL cortex. (A) Excitatory input maps for 13 layer 2/3 (A1) and 12 layer 5 (A2) pyramidal cells each in sham-operated control (left) and FL (right) cortex. Cumulative EPSC amplitudes in individual input maps were averaged and contour lines were derived by linear interpolation. Individual maps were rotated to be parallel to the pia and aligned to the position of the soma on the *x*-axis, and to the border between layer 1 and 2 on the *y*-axis. The color scale represents weak to strong inputs (blue to red), and purple represents activation above the highest level of the regular color scale to emphasize the weaker input patterns, especially in layer 5 control cells. The location of the soma (precise in *x*-axis, approximate in *y*-axis) is indicated by black solid triangles. The numbers and lines at the very left indicate the approximate position of the 6 cortical layers. (*B*) Averaged cumulative inputs for 50 μm rows for cells from control (black) and FL (red) cortex in layer 2/3 (*B1*) and layer 5 (*B2*). (*C*) Average cumulative EPSCs per stimulation site onto layer 2/3 (*C1*) and layer 5 (*C2*) cells originating from layers 2/3, 4/5a, and 5b/6. Input from layer 2/3 and from layer 5b/6 onto layer 5 cells was increased in FL cortex ($P < 0.05$ vs. control). There were no significant changes in layer 2/3 cells from FL cortex, although there was a trend toward increased inputs from layers 2/3 and 4/5a. (*D*) Average activation per stimulation site for each cell. EPSC input was significantly higher in layer 5 cells from FL cortex ($P < 0.01$; *D2*) and did not differ between control and FL cortex in layer 2/3 cells (*D1*). (*E*) Averaged cumulative inputs for 50 μm columns for cells from control (black) and FL (red) cortex in layer 2/3 (*E1*) and layer 5 (*E2*) fitted to Gaussian distributions. The half width of the Gaussian curves did not differ significantly between cells from control and FL cortex. (*F*) Average frequency of sEPSCs and eEPSCs (number of evoked events in the LSPS detection window/window duration, corrected for sEPSC frequency) in layer 2/3 (F1) and layer 5 (F2) pyramidal cells in control (black) and FL (red) cortex. The frequency of spontaneous and evoked EPSC is significantly higher in layer 5 pyramidal cells of FL cortex ($P < 0.05$), but the smaller increase in layer 2/3 cells is not statistically significant. To facilitate comparison of the number of spontaneous versus LSPS-evoked EPSCs, we have converted the number of eEPSCs/stimulated spot (Table 2) into frequency, given the detection window of 45 ms. (*G*) Average amplitudes of spontaneous EPSCs (sEPSCs detected outside of the LSPS window) and evoked EPSCs (eEPSCs, within 5–50 ms of the stimulus) in layer 2/3 (*G1*) and layer 5 (*G2*) pyramidal cells in control (black) and FL (red) cortex. Amplitudes of spontaneous and evoked EPSC do not differ in pyramidal cells of FL cortex.

Table 2
LSPS-evoked and spontaneous EPSCs

	Layer 2/3			Layer 5		
	Sham, $n = 13$	FL, $n = 13$	P	Sham, $n = 12$	FL, $n = 12$	P
LSPS-evoked EPSCs						
Cumulative amplitude/spot (pA)						
From all layers	3.04 ± 0.58	3.92 ± 0.65	—	4.53 ± 0.56	7.56 ± 0.77	**
From layer 2/3	2.47 ± 0.25	3.55 ± 0.70	—	4.23 ± 0.75	7.56 ± 1.53	—
From layer 4/5a	4.10 ± 1.10	5.51 ± 1.05	—	4.23 ± 0.67	4.60 ± 0.39	—
From layer 5/6	2.54 ± 0.58	2.70 ± 0.66	—	5.46 ± 1.11	10.73 ± 2.26	*
Amplitude/kinetics versus number of events[a]						
Amplitude (pA)	9.36 ± 0.68	9.33 ± 0.52	—	10.65 ± 0.88	9.90 ± 0.66	—
90% rise (ms)	1.61 ± 0.04	1.61 ± 0.05	—	1.64 ± 0.07	1.52 ± 0.05	—
Half width (ms)	8.07 ± 0.52	7.75 ± 0.41	—	8.48 ± 0.62	7.11 ± 0.39	—
# of EPSCs/spot	0.621 ± 0.060	0.770 ± 0.020	—	0.546 ± 0.042	0.824 ± 0.034	*
Spontaneous EPSCs						
Amplitude (pA)	7.46 ± 0.52	6.94 ± 0.20	—	7.62 ± 0.53	7.30 ± 0.40	—
90% rise (ms)	1.52 ± 0.03	1.47 ± 0.03	—	1.52 ± 0.04	1.45 ± 0.05	—
Half width (ms)	8.23 ± 0.55	7.71 ± 0.47	—	8.42 ± 0.53	7.40 ± 0.39	—
Frequency (Hz)	10.48 ± 1.22	13.30 ± 1.15	—	8.42 ± 1.39	13.57 ± 2.05	*

Note: Origin and properties of spontaneous and LSPS-evoked EPSCs onto pyramidal cells in FL and sham-operated cortex.
[a]Refers to LSPS-evoked EPSCs from all layers. *$P < 0.05$; **$P < 0.01$; —, not significant, $P > 0.05$.

Spontaneous EPSCs (recorded during acquisition of EPSC input maps in the interstimulation interval starting 0.5 s after photostimulation for 1.5 s/sweep, i.e., totaling ~4 min/cell) showed similar trends in FL animals as LSPS-evoked EPSCs: no changes in amplitude and kinetics (Table 2), an increase in frequency in layer 5 cells (control: 8.42 ± 1.39 Hz., FL: 13.57 ± 2.05 Hz., $P < 0.05$), but no significant increase in frequency in layer 2/3 cells (control: 10.48 ± 1.22 Hz., FL: 13.30 ± 1.15 Hz., $P > 0.1$). The findings regarding spontaneous EPSCs are consistent with previous results (Jacobs and Prince 2005). An

increased number of evoked EPSCs, together with the fact that release probability and intrinsic excitability were unaltered, suggests an increase in recurrent excitatory connectivity via an increase in synapse number. The next experiments were designed to test whether there might be changes in inhibitory connectivity as well.

Layer-Specific Changes in Inhibitory Input onto Pyramidal Cells in FL Cortex

Inhibitory input maps were acquired from the same cells in which excitatory inputs had been mapped. As described in an earlier study (Brill and Huguenard 2009), LSPS can evoke IPSCs with much shorter latency than EPSCs, and these short-latency IPSCs (slIPSCs) frequently have a higher amplitude than longer-latency IPSCs. Additionally, slIPSCs can only be evoked from perisomatic locations, while regular latency IPSCs (rlIPSCs) originate from a wider cortical area. For these reasons, we separated data into IPSCs generated 2–10 ms and 10–50 ms after the LSPS stimulus, slIPSCs and rlIPSCs, respectively. The input maps in Figure 6*A1*,*A2* show cumulative amplitudes of rlIPSCs in layer 2/3 and 5 cells from control and FL cortex. Vertical excitation profiles are shown in Figure 6*B1*,*B2*. The average cumulative IPSC amplitude per stimulated spot was significantly higher in layer 5 cells from FL cortex (control: 3.61 ± 0.48 pA/spot, FL: 5.89 ± 0.86 pA/spot; $P < 0.05$; Fig. 6*D2* and Table 3). In particular, this was due to increased inputs from layer 4/5a (control: 3.87 ± 0.80 pA/spot; FL: 8.65 ± 1.71 pA/spot; $P < 0.05$; Fig. 6*C2*). Layer 2/3 cells in FL and control cortex had similar overall amounts of regular-latency inhibitory input (Fig. 6*D1* and Table 3); however, there was a selective increase in cumulative rlIPSC amplitude originating from layer 4/5a, similar to the results in layer 5 pyramidal cells (control: 0.61 ± 0.13 pA, FL: 1.24 ± 0.23 pA, $P < 0.05$; Fig. 6*C1*).

Amplitude, but Not Number, of rlIPSCs Is Increased in Layer 5 Pyramidal Cells of FL Cortex

We determined whether the increased rlIPSC input onto layer 5 pyramidal cells was due to increases in event amplitude, number, or both. Again, we quantified these parameters for LSPS-evoked (10–50 ms after stimulus) and spontaneous events (recorded during acquisition of IPSC input maps starting 0.5 s after each photostimulation for 1.5 s/sweep). The amplitude of both spontaneous and LSPS-evoked rlIPSCs in layer 5 pyramidal cells from FL cortex was significantly increased (spontaneous: 7.24 ± 0.37 pA vs. 8.54 ± 0.30 pA, $P < 0.05$; LSPS evoked: 11.03 ± 0.88 pA vs. 14.32 ± 1.19 pA, $P < 0.05$; Fig. 6*G2*; Table 3), while IPSC number did not differ significantly (Fig. 6*F2*). Overall rlIPSC frequency and amplitude were unchanged in layer 2/3 pyramidal cells (Fig. 6*F1*,*G1*; Table 2). Increased amplitude, but not number of LSPS-evoked and spontaneous IPSCs, suggests changes in synaptic strength, rather than in the number of inhibitory synapses onto layer 5 pyramidal cells in FL cortex.

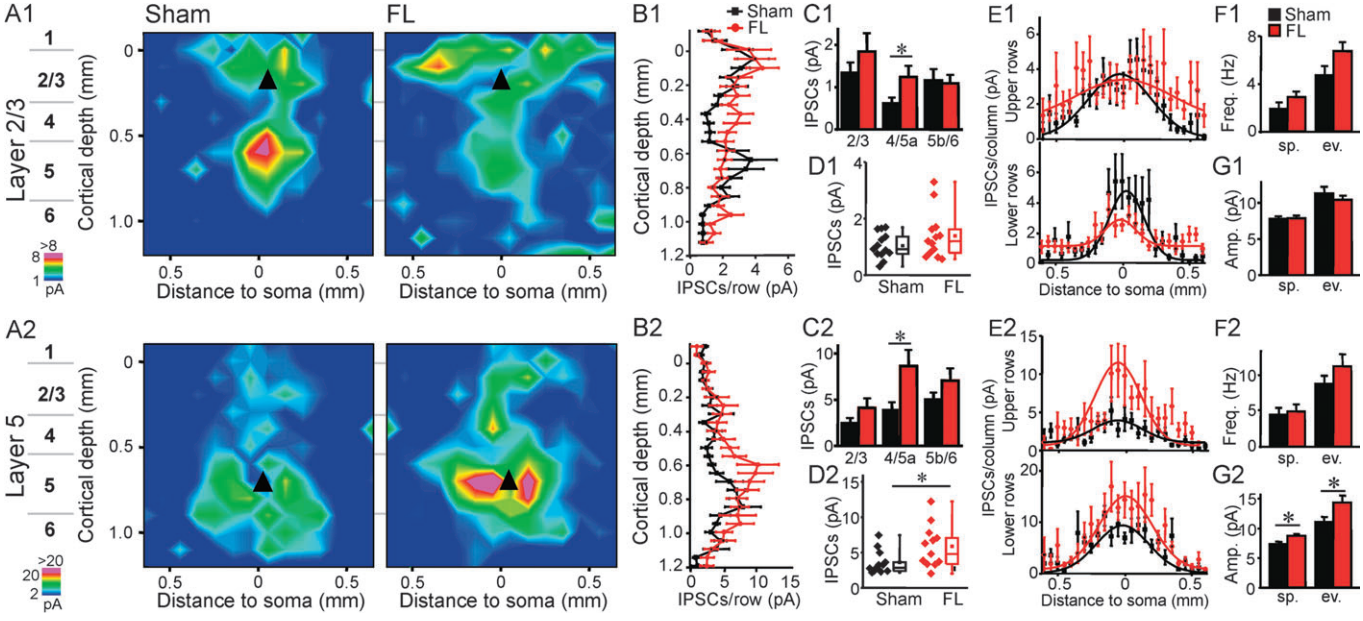

Figure 6. Increased regular latency inhibitory input onto layer 5, but not layer 2/3 cells in FL cortex. (*A*) Averaged input maps for rlIPSCs in 13 layer 2/3 (*A1*) and 12 layer 5 (*A2*) pyramidal cells each in sham-control (left) and FL (right) cortex. Maps were constructed as detailed for Figure 5. (*B*) Averaged inputs for 50 μm rows for cells from control (black) and FL (red) cortex in layer 2/3 (*B1*) and layer 5 (*B2*). The vertical inhibitory profile was altered in the FL for both cell types. Control layer 2/3 cells display a profile with clear peaks in layers 2/3 and 5, while FL 2/3 cells show a profile with a less prominent peak in layer 2/3 and a progressively decreased input in deeper layers. Layer 5 cells, by contrast, receive prominent inputs from layer 5b in control, which is shifted superficially to layer 4/5a in FL cortex. (*C*) Average cumulative rlIPSCs per stimulation site onto layer 2/3 (*C1*) and layer 5 (*C2*) cells originating in layers 2/3, 4/5a, and 5b/6. Input from layer 4/5a onto layer 2/3 and onto layer 5 cells was increased in FL cortex ($P < 0.05$ vs. control for both). (*D*) Average activation per stimulation site for each cell. rlIPSC input was significantly higher in layer 5 cells from FL cortex ($P < 0.05$; *D2*) and did not differ between control and FL cortex in layer 2/3 cells (*D1*). (*E*) Averaged cumulative inputs for 50 μm columns for cells from control (black) and FL (red) cortex in layer 2/3 (*E1*) and layer 5 (*E2*), for upper rows (to cortical depth of 400 μm, mainly layer 2/3) and lower rows. Gaussian fits suggest that input comes from a wider area within upper rows of layer 2/3 cells from FL cortex. (*F*) Average frequency of spontaneous and LSPS-evoked IPSCs in layer 2/3 (*F1*) and layer 5 (*F2*) pyramidal cells in control (black) and FL (red) cortex. The frequency of spontaneous and LSPS-evoked IPSC is not significantly altered in cells from FL cortex. The number of events was converted to frequency given a detection window of 40 ms. (*G*) Average amplitudes of spontaneous IPSCs and LSPS-evoked IPSCs (within 10–50 ms of the stimulus) in layer 2/3 (*G1*) and layer 5 (*G2*) pyramidal cells in control (black) and FL (red) cortex. Amplitudes of spontaneous and LSPS-evoked IPSC were significantly larger in layer 5 pyramidal cells of FL cortex ($P < 0.05$) but did not differ in layer 2/3 cells of sham-control and FL cortex.

Increased slIPSCs in Pyramidal Cells from FL Cortex

Maps of slIPSCs (Fig. 7*A1*,*A2*) revealed significant differences between FL and control cortex in both layers. While slIPSCs were only evoked from perisomatic locations within a similar radius in both control and FL cortex, their cumulative amplitude was significantly increased in both layer 2/3 and 5 cells from the latter (Fig. 7*A*–*C*, Table 3). slIPSCs frequently result from summation of several near-simultaneous individual events (Brill and Huguenard 2009). Therefore, it is often not possible to precisely quantify the number and amplitude of slIPSCs. We did attempt to measure individual events whenever they were distinguishable and found a significantly increased slIPSC amplitude in layer 2/3 cells of FL cortex (control: 27.46 ± 2.01 pA; FL: 37.96 ± 4.01 pA, $P < 0.05$;

Table 3
LSPS-evoked and spontaneous IPSCs

	Layer 2/3			Layer 5		
	Sham, $n = 13$	FL, $n = 13$	P	Sham, $n = 12$	FL, $n = 12$	P
LSPS-evoked rIIPSCs						
Cumulative amplitude/spot (pA)						
From all layers	1.04 ± 1.23	1.39 ± 0.23	—	3.61 ± 0.48	5.89 ± 0.86	*
From layer 2/3	1.34 ± 0.22	1.84 ± 0.42	—	2.46 ± 0.50	4.12 ± 0.94	—
From layer 4/5a	0.61 ± 0.13	1.24 ± 0.23	*	3.87 ± 0.80	8.65 ± 1.71	*
rom layer 5/6	1.16 ± 0.24	1.09 ± 0.17	—	5.03 ± 0.66	7.06 ± 1.26	—
Amplitude/kinetics versus number of events[a]						
Amplitude (pA)	11.27 ± 0.86	10.43 ± 0.56	—	11.03 ± 0.88	14.32 ± 1.19	*
90% rise (ms)	2.26 ± 0.13	2.04 ± 0.10	—	2.05 ± 0.10	1.97 ± 0.13	—
Half width (ms)	36.53 ± 3.27	33.75 ± 2.48	—	26.86 ± 2.57	22.92 ± 3.92	—
rIIPSCs/spot	0.187 ± 0.0029	0.265 ± 0.029	—	0.360 ± 0.046	0.460 ± 0.070	—
LSPS-evoked slIPSC						
Amplitude (pA)	27.46 ± 2.01	37.96 ± 4.01	*	21.68 ± 3.45	30.61 ± 3.78	—
slIPSCs/spot	0.120 ± 0.018	0.145 ± 0.011	—	0.183 ± 0.027	0.229 ± 0.038	—
Spontaneous IPSC						
Amplitude (pA)	7.77 ± 0.33	7.87 ± 0.39	—	7.24 ± 0.37	8.54 ± 0.30	*
90% rise (ms)	1.71 ± 0.07	1.66 ± 0.06	—	1.74 ± 0.05	1.67 ± 0.06	—
Half width (ms)	30.65 ± 2.19	26.91 ± 1.75	—	27.37 ± 2.06	23.01 ± 2.23	—
Frequency (Hz)	1.84 ± 0.49	2.84 ± 0.46	—	4.89 ± 1.07	5.67 ± 1.08	—

Note: Origin and properties of spontaneous and LSPS-evoked rIIPSCs, and of slIPSCs onto pyramidal cells in FL and sham-operated cortex.
[a]Refers to LSPS-evoked EPSCs from all layers. *$P < 0.05$; —, not significant, $P > 0.05$.

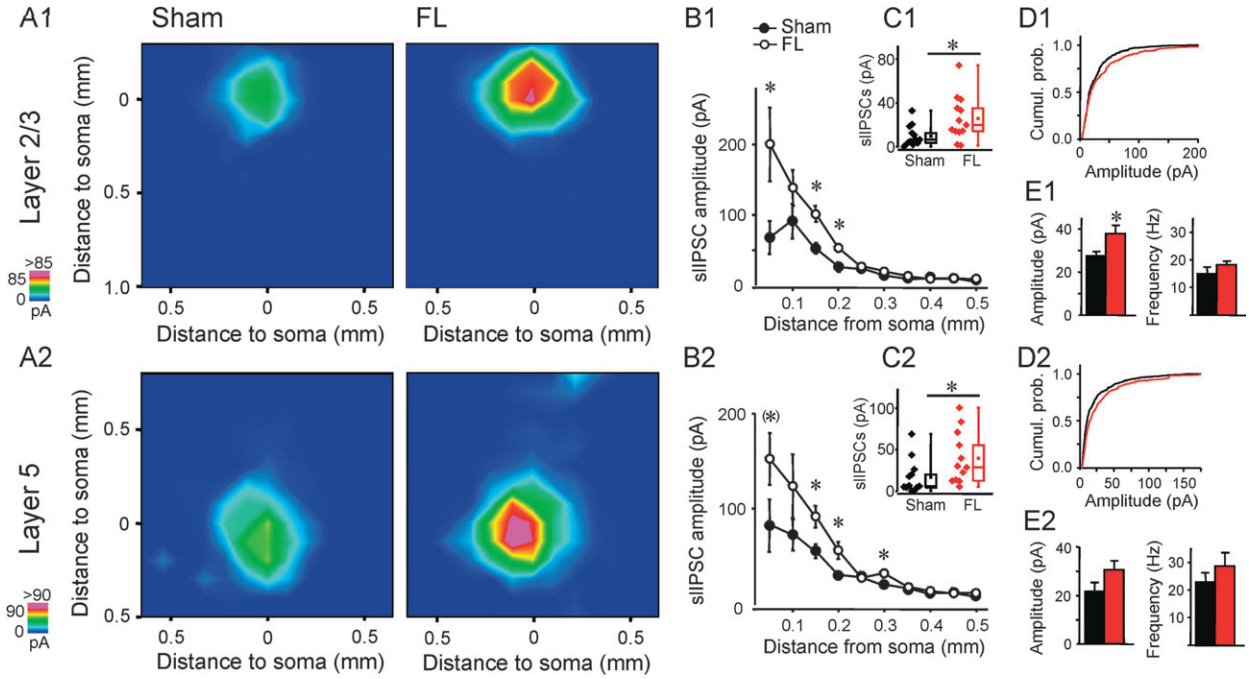

Figure 7. Increased short-latency inhibitory input onto layer 5 and 2/3 cells in FL cortex. (*A*) Input maps for slIPSCs in 13 layer 2/3 (*A1*) and 12 layer 5 (*A2*) pyramidal cells each in sham-control (left) and FL (right) cortex. Averaged maps were constructed as explained for Figure 5, except that maps were aligned to the position of the soma on both the *x*- and *y*-axes. (*B*) Comparison of slIPSC evoked in layer 2/3 (*B1*) and layer 5 cells (*B2*) in control (solid circles) and FL (open circles) cortex. Cumulative amplitudes for each cell were averaged into 50 μm bins according to the distance between stimulation site and the soma. Layer 2/3 and 5 cells received significantly more powerful short-latency PSC input, but it originated from similar cortical areas. (*C*) Average activation per stimulation site within 200 μm of the soma for each cell. slIPSC input was significantly higher in layer 2/3 and 5 cells from FL cortex ($P < 0.05$; *C1* and *C2*, respectively). (*D*) Cumulative probability for amplitudes of slIPSC in layer 2/3 (*D1*) and layer 5 (*D2*) pyramidal cells in control (black) and FL (red) cortex. The curve for cells in FL cortex in both layers is shifted to the right, indicating higher IPSC amplitudes. (*E*) Left panel: average amplitudes of evoked slIPSCs (2–10 ms within stimulus) in layer 2/3 (*E1*) and layer 5 (*E2*) pyramidal cells in control (black) and FL (red) cortex. Right panel: average frequency of slIPSCs in layer 2/3 and 5 pyramidal cells in control (black) and FL (red) cortex. Number of events was converted to frequency given a detection window of 8 ms.

Fig. 7*E1*, Table 3). A similar trend in layer 5 pyramidal cells in FL cortex was seen, but did not reach statistical significance (control: 21.68 ± 3.45 pA; FL: 30.61 ± 3.78 pA, $P > 0.05$; Fig. 7*E2*, Table 3).

Comparison between Excitatory and Inhibitory Input

To assess how changes in excitatory and inhibitory input relate to each other, we compared the cumulative amplitude ratios for rlIPSCs and EPSCs originating in layer 2/3, 4/5a, and 5b/6 within each cell (Fig. 8). Not surprisingly, in layer 2/3 cells—where no significant changes in overall EPSC and rlIPSC input had been observed—there were no significant changes in EPSC:rlIPSC ratios (Fig. 8*A*). In layer 5 pyramidal cells, we found significantly smaller EPSC:rlIPSC ratios in FL cortex (from layer 4/5a; control: 1.35 ± 0.27; FL: 0.72 ± 0.11; $n = 12$ each; $P < 0.05$), reflecting the stronger rlIPSC input from these layers (Fig. 8*B*).

Discussion

We investigated monosynaptic excitatory (AMPA/kainate receptor mediated) and inhibitory ($GABA_A$ receptor mediated) inputs onto pyramidal cells in layers 2/3 and 5 of rat primary somatosensory cortex in the FL model of cortical dysplasia. Freeze-lesioning within 48 h of birth (Dvorak and Feit 1977) results in the death of cortical neurons that are present at that time, that is, those in layers 4–6. Subsequently, a 4-layered structure forms that is histopathologically similar to human 4-layered microgyria (Dvorak et al. 1978). Unlike humans with this type of dysplasia, rats with a single FL do not experience spontaneous seizures (Kellinghaus et al. 2007), although they have a decreased threshold for hyperthermia-induced seizures (Scantlebury et al. 2004) and cortical slice preparations display hyperexcitability. Humans typically have multiple such lesions, while usually only one FL is induced in rats, which might account for this difference. In slice preparations, the normally laminated region lateral of the microgyrus remains hyperexcitable even when the gyrus has been separated prior to recording (Jacobs et al. 1996). In human polymicrogyria, epileptiform activity may likewise originate from the region outside of the microgyri (Chassoux et al. 2008). In this study, we examined monosynaptic inputs onto pyramidal cells in the hyperexcitable region approximately 0.5–1.0 mm lateral to the edge of the microgyrus and compared it with equivalent cortical areas in sham-operated control rats.

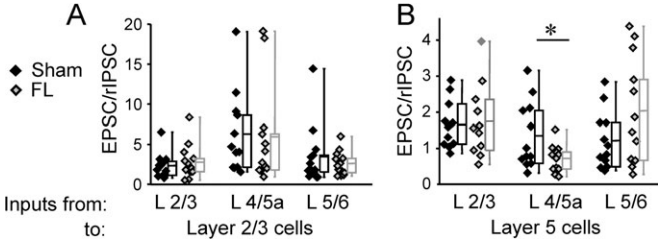

Figure 8. Comparison of excitatory and inhibitory activation. (*A*) EPSC:rlIPSC ratios from each layer 2/3 cell mapped in FL (black diamonds) and sham-control (gray diamonds) cortex, for inputs originating in layer 2/3, 4/5a, and 5b/6. There were no significant differences between cells from FL and control cortex. (*B*) Same as (*A*), for layer 5 cells. Ratios representing inputs from layer 4/5a differed significantly between cells from FL and control cortex ($P < 0.05$), reflecting the increased rlIPSC input from that region.

Using LSPS, we examined the following parameters: excitation profiles (i.e., action potential output in the stimulated cells resulting from LSPS), direct glutamatergic currents in the recorded cells, monosynaptic excitatory inputs, and 2 types of monosynaptic inhibitory inputs, that is, slIPSCs, largely from FS interneurons (basket and/or chandelier cells [Brill and Huguenard 2009]), and rlIPSCs, largely from non-FS interneurons. Excitation profiles, direct glutamatergic activation, intrinsic excitability, and short-term excitatory synaptic plasticity did not differ between pyramidal cells from FL and control cortex. LSPS-evoked excitatory inputs onto layer 5 pyramidal cells were increased in FL cortex. The increase was due to a larger number of LSPS-evoked EPSCs onto layer 5 pyramidal cells per stimulation site without any change in amplitude, consistent with an earlier study of spontaneous EPSCs (Jacobs and Prince 2005). LSPS-evoked EPSCs onto layer 2/3 pyramidal cells in FL cortex did not differ significantly from control. LSPS input maps in cells from sham-control animals were qualitatively similar to published input maps (Jin et al. 2006; Xu and Callaway 2009). Layer 2/3 and 5 cells also received increased rlIPSC input from layer 4 and 5a. Unlike the EPSC increase, this increase was due to changes in IPSC amplitude rather than number of IPSCs, suggesting changes in synaptic strength. Cells in both layers received significantly increased slIPSC input.

The increase in EPSC frequency in the absence of changes in intrinsic excitability or release probability can be explained by axonal sprouting, a phenomenon frequently observed in hyperexcitable tissue. It involves the formation of new axon collaterals that synapse onto new targets, thus remodeling neuronal microcircuits (Sutula et al. 1989; Salin et al. 1995; Represa et al. 2008; reviewed in Ben Ari 2006). Alternatively, it could be due to defects in synapse elimination resulting in an increased number of dendritic spines (Zhou et al. 2009b; reviewed in Yoshihara et al. 2009) or an increased connection probability between pyramidal cells. Increased recurrent excitatory connections can underlie network hyperexcitability. Longer basal dendrites are present in layer 5 corticothalamic pyramidal cells in approximately 3 months old FL rats, while layer 3 corticocortical cells have a simplified dendritic branching pattern and fewer spines (Di Rocco et al. 2001, 2002). Although these studies were done in much older rats, they are in agreement with the results presented here.

In contrast to the FL-associated changes in synaptic excitation we observed, the increase in inhibitory connectivity is unlikely to arise from sprouting and/or deficient pruning. Previous reports have not demonstrated consistent changes in the number of interneurons in cortical tissue surrounding FLs. Data by Schwarz et al. (2000) and Hablitz and DeFazio (1998) show unaltered numbers of parvalbumin-positive (i.e., fast spiking) interneurons medial and lateral to the lesion (although Rosen et al. (1998) report selective decreases in parvalbumin-positive neurons in infragranular layers adjacent to the lesion). The number of somatostatin-containing interneurons is decreased slightly in rats older than P30 (Patrick et al. 2006). The number of calbindin-positive cells proximal to the lesion is increased, but the overall number of γ-aminobutyric acid (GABA)-containing neurons is unaltered (Schwarz et al. 2000). In apparent contradiction to this, widespread decreases in GABA-binding sites (Zilles et al. 1998) and $GABA_A$ receptor expression (Redecker et al. 2000) have been observed in FL cortex. Reconciling decreases in GABA binding and $GABA_A$ receptor expression with grossly unaltered interneuronal

counts and increased IPSC amplitudes will require further study. Changes in inhibitory connectivity may stem from changes in synaptic strength that might result from either pre- or postsynaptic mechanisms. Potential causes include changes in receptor subtype expression (DeFazio and Hablitz 1999; Loup et al. 2006), changes in the dynamics of GABA receptor surface expression and internalization (Kittler et al. 2000; Goodkin et al. 2007; Michels and Moss 2007), or increased quantal size (Hartmann et al. 2008). Consistent with the idea of postsynaptic changes and with our findings reported here, miniature IPSCs in layer 2/3 pyramidal cells in FL cortex have increased amplitudes, but unaltered frequency and their sensitivity to zolpidem is decreased, which suggests changes in $GABA_A$ receptor subunit expression (DeFazio and Hablitz 1999). A different study (Jacobs and Prince 2005) showed increased peak conductance, but not frequency, of spontaneous IPSCs in layer 5 pyramidal cells. However, this was likely due to increased excitatory drive onto interneurons, since the differences disappeared when action potentials or glutamatergic neurotransmission were blocked. The discrepancy to our results might be explained by regional differences: Jacobs and Prince (2005) recorded from cells closer to, and both lateral and medial of, the lesion, while we recorded only lateral of the microgyrus.

Overall EPSC and rlIPSC inputs onto layer 5 cells in FL cortex were significantly increased, but those onto layer 2/3 cells were less severely affected. At the time of freeze-lesioning (P0), cortical layers 4–6 have already formed and are thus destroyed by freeze-lesioning. Connectivity within the anatomically normal, but ultimately electrophysiologically hyperexcitable, region surrounding the lesion might compensate for the disruption at the site of the lesion. Layer 2/3 forms after lesioning and an anatomically aberrant but contiguous layer is present across the lesion (Rosen et al. 1996; Nadarajah et al. 2002). The hyperconnectivity in layer 5 and the more normal connectivity pattern in layer 2/3 of FL cortex might reflect this fact: layer 5 cells surrounding the lesion are deprived of their intralaminar connections at the lesion and form an increased number of recurrent connections with cells outside the lesion. In contrast, layer 2/3 cells migrate to their final laminar destination after the insult and do not lose their intralaminar "partners." However, their infragranular partners in and around the lesion are absent; thus, they may form exuberant connections onto surviving layer 5 pyramidal neurons, which is consistent with the enhanced inputs from layer 2/3 onto layer 5 that we observed (Fig. 5*B2*,*C2*). Additionally, layer 2/3 EPSCs showed a consistent but ultimatively not statistically significant trends toward an increased numbers of spontaneous and LSPS-evoked EPSCs and increased inputs from layer 4/5a. Taken together, this does not rule out subtle increases in connectivity that are qualitatively similar to those seen in layer 5 cells.

Despite simultaneous increases in both excitatory and inhibitory local intracortical connectivity demonstrated here, cortical slices from FL rats are hyperexcitable (Jacobs et al. 1999a). This may result from a number of factors. For example, the functional changes in excitation and inhibition may not be balanced. In addition, our methods do not provide information regarding long-range excitatory connectivity from callosal and/or thalamocortical projections that converge onto the paramicrogyral region (Jacobs et al. 1999b; Rosen et al., 2000). LSPS, which induces spike generation by stimulating the somata of presynaptic neurons (unlike electrical stimulation which excites axons), likely undersamples long-range excitatory inputs compared with the more short-range inhibitory inputs.

FS interneurons, whose inputs give rise to slIPSCs (Brill and Huguenard 2008), comprise basket cells and chandelier cells, and it will be important in the future to determine whether synapses of these two cell types onto pyramidal cells are regulated in the same way. FS interneurons provide strong, fast, and robust inhibition (Thomson et al. 1996; Xiang et al. 2002) and might therefore inhibit the initiation or spread of epileptiform network activation (Lau et al. 2000; Gibson et al. 2008). On the other hand, strong recruitment of FS interneurons can enhance network synchronization (Fuchs et al. 2007) and might thus be proepileptic under certain conditions. Similarly, chandelier cells might cause pyramidal cell excitation due to the depolarized chloride equilibrium potential in axon initial segments (Szabadics et al. 2006). In addition, chandelier cells show relatively larger increases in activity than other interneuron types during intense excitation, suggesting that their output might critically regulate seizure activity (Zhu et al. 2004). In either scenario, FS interneurons would be critically involved in shaping epileptiform activity. Non-FS interneurons, whose synapses mainly target dendrites, can likewise influence network activity by phase shifting dendritic spiking in pyramidal cells (Kim et al. 1995). Enhanced rlIPSCs might therefore also shape epileptiform network responses in FL cortex. The specific enhancement of rlIPSC connectivity from layer 4/5a onto both layers 2/3 and 5 pyramidal cells shows that presumed non-FS dendritically targeting interneurons in this thalamorecipient layer are specifically affected by the connectivity changes in FL cortex.

Our studies do not address whether the observed changes in EPSC and IPSC input in FL cortex are primary or compensatory. A possible scenario might be that axonal sprouting results in increased excitatory drive onto pyramidal cells (Jacobs and Prince 2005). Upregulation of the strength of inhibitory synapses onto pyramidal cells would then serve to compensate for the increased excitatory drive (see Supplementary Figure 1). EPSC frequency in FL cortex is already significantly increased over controls at P10, approximately 2 days before epileptiform field potentials can be evoked (Jacobs et al. 1999a; Zsombok and Jacobs 2007), suggesting that excitatory hyperconnectivity may be the initial factor. Miniature EPSC frequency specifically onto FS interneurons appears to be decreased (K. Jacobs, personal communication). Thus, upregulation of synaptic output of FS onto pyramidal cells (i.e., increased slIPSCs) might be a homeostatic mechanism to maintain output despite the decreased input. Hyperexcitability in cortical malformations (Aronica et al. 2007; Munakata et al. 2007) and other pathological situations may be accompanied by changes in chloride homeostasis, which may result in $GABA_A$-receptor mediated depolarization. Such excitatory GABA responses usually result from alterations in expression of the chloride cotransporter KCC2 and/or the sodium-potassium-chloride cotransporter NKCC1 (reviewed in Ben-Ari et al. 2007). Obviously, changes in chloride reversal potential need to be taken into consideration when analyzing the properties of neuronal networks. However, KCC2 and NKCC1 expression in freeze-lesioned cortex of rats after P14 does not differ from control cortex (Shimizu-Okabe et al. 2007), suggesting that GABAergic IPSCs are inhibitory.

Although electrographic seizures in vivo are rare in many animal models of cortical dysplasia (reviewed in Wong 2009), dysplastic cortex is usually characterized by changes in the relative weight of excitation and inhibition. Hippocampal CA1 pyramidal cells in Lis1 heterozygous mice, a model for lissencephaly, have an increased number of spontaneous and miniature EPSCs without changes in amplitude or kinetics (Greenwood et al. 2009a) and increased excitatory drive onto interneurons (Jones and Baraban 2007), similar to layer 5 pyramidal cells in FL cortex. Cortical dysplasia induced by in utero irradiation causes cortical hyperexcitability (Roper et al. 1997) and decreases IPSC and EPSC frequencies in cortical interneurons, resulting in a net disinhibition (Zhou et al. 2009a). Prenatal exposure to methylazoxymethanol acetate reduces seizure threshold (Chevassus-au-Louis et al. 1998) and alters intracortical and intrahippocampal connectivity (Chevassus-au-Louis et al. 1999). Taken together, synaptic reorganization causes changes in excitatory and inhibitory inputs onto principal and interneurons in cortical dysplasia models, although the precise nature of these alterations varies between models.

Our investigation of excitatory and inhibitory connectivity in FL cortex yielded 3 main results: firstly, upregulation of EPSCs and rIIPSCs is due to different mechanisms: while an increased event "frequency" underlies the enhancement of excitatory connectivity, regular latency inhibitory input is augmented due to increased event "amplitudes." Secondly, FS to pyramidal cell input is specifically enhanced in FL cortex (see Supplementary Figure 1). The increases in excitatory and inhibitory inputs provide a possible explanation why FL animals do not exhibit overt seizures. Thirdly, we show that layer 2/3 pyramidal cells are less affected than those in layer 5, which correlates with the fact that layer 5 forms before and layer 2/3 forms after lesioning. Together, these findings delineate parallel mechanisms that regulate excitability in the developing neocortex.

Supplementary Material

Supplementary material can be found at: http://www.cercor.oxfordjournals.org/

Funding

National Institute of Neurological Disorders and Stroke (NS12151 to J.R.H.); American Epilepsy Society postdoctoral fellowship to J.B.

Notes

We would like to thank Dr David Prince for helpful discussions and critical reading of an earlier version of the manuscript and Isabel Parada for technical assistance. *Conflict of Interest*: None declared.

References

Aronica E, Boer K, Redeker S, Spliet WG, van Rijen PC, Troost D, Gorter JA. 2007. Differential expression patterns of chloride transporters, Na+-K+-2Cl–cotransporter and K+-Cl–cotransporter, in epilepsy-associated malformations of cortical development. Neuroscience. 145:185–196.

Barkovich AJ, Lindan CE. 1994. Congenital cytomegalovirus-infection of the brain—imaging analysis and embryologic considerations. Am J Neuroradiol. 15:703–715.

Barkovich AJ, Rowley H, Bollen A. 1995. Correlation of prenatal events with the development of polymicrogyria. Am J Neuroradiol. 16:822–827.

Ben Ari Y. 2006. Basic developmental rules and their implications for epilepsy in the immature brain. Epileptic Disord. 8:91–102.

Ben-Ari Y, Gaiarsa JL, Tyzio R, Khazipov R. 2007. GABA: a pioneer transmitter that excites immature neurons and generates primitive oscillations. Physiol Rev. 87:1215–1284.

Brill J, Huguenard JR. 2008. Sequential changes in AMPA receptor targeting in the developing neocortical excitatory circuit. J Neurosci. 28:13918–13928.

Brill J, Huguenard JR. 2009. Robust short-latency perisomatic inhibition onto neocortical pyramidal cells detected by laser-scanning photostimulation. J Neurosci. 29:7413–7423.

Busetto G, Higley MJ, Sabatini BL. 2008. Developmental presence and disappearance of postsynaptically silent synapses on dendritic spines of rat layer 2/3 pyramidal neurons. J Physiol. 586:1519–1527.

Chassoux F, Landre E, Rodrigo S, Beuvon F, Turak B, Semah F, Devaux B. 2008. Intralesional recordings and epileptogenic zone in focal polymicrogyria. Epilepsia. 49:51–64.

Chevassus-au-Louis N, Ben-Ari Y, Vergnes M. 1998. Decreased seizure threshold and more rapid rate of kindling in rats with cortical malformation induced by prenatal treatment with methylazoxymethanol. Brain Res. 812:252–255.

Chevassus-au-Louis N, Jorquera I, Ben-Ari Y, Represa A. 1999. Abnormal connections in the malformed cortex of rats with prenatal treatment with methylazoxymethanol may support hyperexcitability. Dev Neurosci. 21:385–392.

Crino PB. 2004. Malformations of cortical development: molecular pathogenesis and experimental strategies. Adv Exp Med Biol. 548:175–191.

DeFazio RA, Hablitz JJ. 1999. Reduction of zolpidem sensitivity in a freeze lesion model of neocortical dysgenesis. J Neurophysiol. 81:404–407.

Deleuze C, Huguenard JR. 2006. Distinct electrical and chemical connectivity maps in the thalamic reticular nucleus: potential roles in synchronization and sensation. J Neurosci. 26:8633–8645.

Destexhe A, Contreras D, Steriade M, Sejnowski TJ, Huguenard JR. 1996. In vivo, in vitro, and computational analysis of dendritic calcium currents in thalamic reticular neurons. J Neurosci. 16:169–185.

Di Rocco F, Giannetti S, Gaglini P, Di Rocco C, Granato A. 2001. Dendritic anomalies in a freezing model of microgyria: a parametric study. Pediatr Neurosurg. 34:57–62.

Di Rocco F, Giannetti S, Gaglini P, Di Rocco C, Granato A. 2002. Dendritic architecture of corticothalamic neurons in a rat model of microgyria. Childs Nerv Syst. 8:690–693.

Dvorak K, Feit J. 1977. Migration of neuroblasts through partial necrosis of cerebral-cortex in newborn rats contribution to problems of morphological development and developmental period of cerebral microgyria—histological and autoradiographical study. Acta Neuropathol. 38:203–212.

Dvorak K, Feit J, Jurankova Z. 1978. Experimentally induced focal microgyria and status verrucosus deformis in rats—pathogenesis and interrelation histological and autoradiographical study. Acta Neuropathol. 44:121–129.

Fuchs EC, Zivkovic AR, Cunningham MO, Middleton S, Lebeau FEN, Bannerman DM, Rozov A, Whittington MA, Traub RD, Rawlins JNP, et al. 2007. Recruitment of parvalbumin-positive interneurons determines hippocampal function and associated behavior. Neuron. 53:591–604.

Gibson JR, Bartley AF, Hays SA, Huber KM. 2008. Imbalance of neocortical excitation and inhibition and altered UP states reflect network hyperexcitability in the mouse model of fragile X syndrome. J Neurophysiol. 100:2615–2626.

Goodkin HP, Sun CS, Yeh JL, Mangan PS, Kapur J. 2007. GABA(A) receptor internalization during seizures. Epilepsia. 48:109–113.

Greenwood JS, Wang Y, Estrada RC, Ackerman L, Ohara PT, Baraban SC. 2009. Seizures, enhanced excitation, and increased vesicle number in Lis1 mutant mice. Ann Neurol. 66:644–653.

Hablitz JJ, DeFazio T. 1998. Excitability changes in freeze-induced neocortical microgyria. Epilepsy Res. 32:75–82.

Hagemann G, Kluska MM, Redecker C, Luhmann HJ, Witte OW. 2003. Distribution of glutamate receptor subunits in experimentally induced cortical malformations. Neuroscience. 117:991–1002.

Harding B, Copp AJ. 1997. Malformations. In: Graham DI, Lantos PL, editors. Greenfield's neuropathology. 6th ed. London: Arnold. p. 397–533.

Hartmann K, Bruehl C, Golovko T, Draguhn A. 2008. Fast homeostatic plasticity of inhibition via activity-dependent vesicular filling. PLoS ONE. 3:e2979.

Hutsler JJ, Lee DG, Porter KK. 2005. Comparative analysis of cortical layering and supragranular layer enlargement in rodent carnivore and primate species. Brain Res. 1052:71–81.
Isaac JTR, Crair MC, Nicoll RA, Malenka RC. 1997. Silent synapses during development of thalamocortical inputs. Neuron. 18:269–280.
Jacobs KM, Gutnick MJ, Prince DA. 1996. Hyperexcitability in a model of cortical maldevelopment. Cereb Cortex. 6:514–523.
Jacobs KM, Hwang BJ, Prince DA. 1999a. Focal epileptogenesis in a rat model of polymicrogyria. J Neurophysiol. 81:159–173.
Jacobs KM, Mogensen M, Warren E, Prince DA. 1999b. Experimental microgyri disrupt the barrel field pattern in rat somatosensory cortex. Cereb Cortex. 9:733–744.
Jacobs KM, Prince DA. 2005. Excitatory and inhibitory postsynaptic currents in a rat model of epileptogenic microgyria. J Neurophysiol. 93:687–696.
Jin XM, Prince DA, Huguenard JR. 2006. Enhanced excitatory synaptic connectivity in layer V pyramidal neurons of chronically injured epileptogenic neocortex in rats. J Neurosci. 26:4891–4900.
Jones DL, Baraban SC. 2007. Characterization of inhibitory circuits in the malformed hippocampus of Lis1 mutant mice. J Neurophysiol. 98:2737–2746.
Kellinghaus C, Moddel G, Shigeto H, Ying Z, Jacobsson B, Gonzalez-Martinez J, Burrier C, Janigro D, Najm IM. 2007. Dissociation between in vitro and in vivo epileptogenicity in a rat model of cortical dysplasia. Epileptic Disord. 9:11–19.
Kim HG, Beierlein M, Connors BW. 1995. Inhibitory control of excitable dendrites in neocortex. J Neurophysiol. 74:1810–1814.
Kittler JT, Delmas P, Jovanovic JN, Brown DA, Smart TG, Moss SJ. 2000. Constitutive endocytosis of GABA(A) receptors by an association with the adaptin AP2 complex modulates inhibitory synaptic currents in hippocampal neurons. J Neurosci. 20:7972–7977.
Lau D, Vega-Saenz de Miera E, Contreras D, Ozaita A, Harvey M, Chow A, Noebels JL, Paylor R, Morgan JI, Leonard CS, et al. 2000. Impaired fast-spiking, suppressed cortical inhibition, and increased susceptibility to seizures in mice lacking Kv3.2 K+ channel proteins. J Neurosci. 20:9071–9085.
Leventer RJ, Guerrini R, Dobyns WB. 2008. Malformations of cortical development and epilepsy. Dialogues Clin Neurosci. 10:47–62.
Loup F, Picard F, Andre VM, Kehrli P, Yonekawa Y, Wieser HG, Fritschy JM. 2006. Altered expression of alpha 3-containing GABA(A) receptors in the neocortex of patients with focal epilepsy. Brain. 129:3277–3289.
Luhmann HJ, Karpuk N, Qu M, Zilles K. 1998. Characterization of neuronal migration disorders in neocortical structures. II. Intracellular in vitro recordings. J Neurophysiol. 80:92–102.
Luhmann HJ, Raabe K. 1996. Characterization of neuronal migration disorders in neocortical structures.1. Expression of epileptiform activity in an animal model. Epilepsy Res. 26:67–74.
Michels G, Moss SJ. 2007. GABA(A) receptors: properties and trafficking. Crit Rev Biochem Mol Biol. 42:3–14.
Munakata M, Watanabe M, Otsuki T, Nakama H, Arima K, Itoh M, Nabekura J, Iinuma K, Tsuchiya S. 2007. Altered distribution of KCC2 in cortical dysplasia in patients with intractable epilepsy. Epilepsia. 48:837–844.
Nadarajah B, Alifragis P, Wong ROL, Parnavelas JG. 2002. Ventricle-directed migration in the developing cerebral cortex. Nat Neurosci. 5:218–224.
Pang T, Atefy R, Sheen V. 2008. Malformations of cortical development. Neurologist. 14:181–191.
Patrick SL, Connors BW, Landisman CE. 2006. Developmental changes in somatostatin-positive interneurons in a freeze-lesion model of epilepsy. Epilepsy Res. 70:161–171.
Redecker C, Luhmann HJ, Hagemann G, Fritschy JM, Witte OW. 2000. Differential downregulation of GABA(A) receptor subunits in widespread brain regions in the freeze-lesion model of focal cortical malformations. J Neurosci. 20:5045–5053.
Represa A, Tremblay E, Ben-Ari Y. 2008. Sprouting of mossy fibers in the hippocampus of epileptic human and rat. Adv Exp Med Biol. 268:419–424.
Roper SN, King MA, Abraham LA, Boillot MA. 1997. Disinhibited in vitro neocortical slices containing experimentally induced cortical dysplasia demonstrate hyperexcitability. Epilepsy Res. 26:443–449.
Rosen GD, Burstein D, Galaburda AM. 2000. Changes in efferent and afferent connectivity in rats with induced cerebrocortical microgyria. J Comp Neurol. 418:423–440.
Rosen GD, Jacobs KM, Prince DA. 1998. Effects of neonatal freeze lesions on expression of parvalbumin in rat neocortex. Cereb Cortex. 8:753–761.
Rosen GD, Press DM, Sherman GF, Galaburda AM. 1992. The development of induced cerebrocortical microgyria in the rat. J Neuropathol Exp Neurol. 51:601–611.
Rosen GD, Sherman GF, Galaburda AM. 1996. Birthdates of neurons in induced microgyria. Brain Res. 727:71–78.
Rumpel S, Kattenstroth G, Gottmann K. 2004. Silent synapses in the immature visual cortex: layer-specific developmental regulation. J Neurophysiol. 91:1097–1101.
Salin P, Tseng GF, Hoffman S, Parada I, Prince DA. 1995. Axonal sprouting in layer V pyramidal neurons of chronically injured cerebral cortex. J Neurosci. 15:8234–8245.
Scantlebury MH, Ouellet PL, Psarropoulou C, Carmant L. 2004. Freeze lesion-induced focal cortical dysplasia predisposes to atypical hyperthermic seizures in the immature rat. Epilepsia. 45:592–600.
Schwarz P, Stichel CC, Luhmann HJ. 2000. Characterization of neuronal migration disorders in neocortical structures: loss or preservation of inhibitory interneurons? Epilepsia. 41:781–787.
Shimizu-Okabe C, Okabe A, Kilb W, Sato K, Luhmann HJ, Fukuda A. 2007. Changes in the expression of cation-Cl- cotransporters, NKCC1 and KCC2, during cortical malformation induced by neonatal freeze-lesion. Neurosci Res. 59:288–295.
Sisodiya SM. 2004. Malformations of cortical development: burdens and insights from important causes of human epilepsy. Lancet Neurol. 3:29–38.
Sutula T, Cascino G, Cavazos J, Parada I, Ramirez L. 1989. Mossy fiber synaptic reorganization in the epileptic human temporal-lobe. Ann Neurol. 26:321–330.
Szabadics J, Varga C, Molnar G, Olah S, Barzo P, Tamas G. 2006. Excitatory effect of GABAergic axo-axonic cells in cortical microcircuits. Science. 311:233–235.
Thomson AM, West DC, Hahn J, Deuchars J. 1996. Single axon IPSPs elicited in pyramidal cells by three classes of interneurones in slices of rat neocortex. J Physiol. 496:81–102.
Wong M. 2009. Animal models of focal cortical dysplasia and tuberous sclerosis complex: recent progress toward clinical applications. Epilepsia 50 Suppl 9:34–44.
Xiang ZX, Huguenard JR, Prince DA. 2002. Synaptic inhibition of pyramidal cells evoked by different interneuronal subtypes in layer V of rat visual cortex. J Neurophysiol. 88:740–750.
Xu X, Callaway EM. 2009. Laminar specificity of functional input to distinct types of inhibitory cortical neurons. J Neurosci. 29:70–85.
Yoshihara Y, De Roo M, Muller D. 2009. Dendritic spine formation and stabilization. Curr Opin Neurobiol. 19:146–153.
Zhou FW, Chen HX, Roper SN. 2009a. Balance of inhibitory and excitatory synaptic activity is altered in fast-spiking interneurons in experimental cortical dysplasia. J Neurophysiol. 102:2514–2525.
Zhou YD, Lee S, Jin Z, Wright M, Smith SE, Anderson MP. 2009b. Arrested maturation of excitatory synapses in autosomal dominant lateral temporal lobe epilepsy. Nat Med. 15:1208–1214.
Zhu Y, Stornetta RL, Zhu JJ. 2004. Chandelier cells control excessive cortical excitation: characteristics of whisker-evoked synaptic responses of layer 2/3 nonpyramidal and pyramidal neurons. J Neurosci. 24:5101–5108.
Zilles K, Qu M, Schleicher A, Luhmann HJ. 1998. Characterization of neuronal migration disorders in neocortical structures: quantitative receptor autoradiography of ionotropic glutamate, GABA(A), and GABA(B) receptors. Eur J Neurosci. 10:3095–3106.
Zsombok A, Jacobs KM. 2007. Postsynaptic currents prior to onset of epileptiform activity in rat microgyria. J Neurophysiol. 98:178–186.